Available online at www.sciencedirect.com

ScienceDirect

IFAC PapersOnLine 54-16 (2021) 402–409

An Underwater Photogrammetric Application to Generate Micro-Bathymetry Data for Benthic Habitat Mapping and Analysis at Arctic Ocean

Amin Mardani Nejad*. Thomas Luhmann*. Thomas P. Kersten. Boris Dorschel***. Autun Purser*****

* *Jade University, Institute for Applied Photogrammetry and Geoinformatics (IAPG), Ofener Straße 16/19 D-26121 Oldenburg, Germany (e-mail: amin.mardani-nejad@jade-hs.de & luhmann@jade-hs.de).*

** *HafenCity University Hamburg (HCU), Henning-Voscherau-Platz 1, D-20457 Hamburg, (e-mail: thomas.kersten@hcu-hamburg.de)*

*** *Alfred Wegener Institute for Polar and Marine Research (AWI), Van-Ronzelen-Str. 2, Am Handelshafen 12, D-27570 Bremerhaven (e-mail: boris.dorschel@awi.de, autun.purser@awi.de)*

Abstract: The Ocean Floor Observation and Bathymetry System (OFOBS) is an underwater survey platform, which is designed and developed for research in the Polar Regions by the Alfred Wegener Institute (AWI). The tailored deep tow system brought a new perspective and clarity from Arctic Ocean by its optical and acoustic sensors. During the PS101 expedition at the Karasik seamount, OFOBS provides a novel picture of megafauna's habitats. In this study, we develop a methodology to convert the imagery dataset to micro-bathymetry in order to provide primary data for object detection and habitat mapping which will provide a better understanding of arctic benthic habitats. The methodology is based on the underwater photogrammetry workflow and two different point cloud classification methods adopted for sponge detection in 3D point clouds, to facilitate habitat mapping with a focus on the central of Karasik seamount where an extensive and dense assemblage of the Geodia sponges is dominating the seafloor.

Keywords: Underwater photogrammetry, bathymetry, point cloud classification, feature detection, benthic habitat mapping, structure from motion (SfM), Geodia sponges.

1. INTRODUCTION

The largest ecosystem on Earth, which covers approximately 65% of the Earth surface, is the Benthic deep-sea environment (Danovaro et al. 2017). Despite this, only a small fraction of the world's ocean floors has been surveyed using multibeam echo sounders to date. The existing bathymetry data is mainly derived from the satellite altimetry and gravimetry, employed in the General Bathymetric Chart of the Oceans (GEBCO), which includes the Bathymetric Chart of the Arctic Ocean (IBCAO). During the RV Polarstern PS101 expedition, one of the objectives was to collect multibeam bathymetry data, to contribute and improve upon the existing ocean datasets. A key aim was also to study the megabenthos on the Karasik seamount summit and flanks, by the means of analysing the distribution, diversity and production of fauna along depth gradients from the central seamount peak (Boetius and Purser 2017). In order to study this phenomenon the recently developed deep tow system, developed by the Alfred Wegener Institute, was employed for data acquisition. The Ocean Floor Observation and Bathymetry System (OFOBS) for deep-sea research has a variety of optical and bathymetry sensors, as well as underwater navigation systems which work in parallel with the support of the vessel navigation sensors. In this study, we developed an underwater photogrammetry workflow (based on an existing OFOBS imagery dataset), for object detection, which utilised and tested two different methods of point cloud classification in order to provide fundamental geospatial information for high resolution habitat mapping and analyses. In order to investigate the benthic habitat characteristics of the study area, the Geodia sponge was chosen as the target of feature detection. The other ecosystem community members, such as starfish and shrimp were not targeted in this study.

2. BASIC PRINCIPLES AND BACKGROUND INFORMATION

2.1 Habitat mapping of benthos

The term 'benthic community' refers to those marine organisms which live at the ocean floor interface, within the bottom meters of ocean, directly on or within the marine sediments; this community is also known as the benthos. The main groups within the benthos at the study site are shrimps, clams, lobsters, crabs, sponges and worms, though these may significantly change with each region. Sponges are active filter feeders, sessile and of importance to other fauna as their form provides structurally complex habitats for other benthos, fish and invertebrates to utilize, therefore enhancing local biodiversity (Keegan et al. 1976). Benthic habitat studies based on geospatial information are required to provide a premier understanding of the distribution and extent of diverse marine ecologies. As a multidisciplinary term, benthic habitat mapping covers a wide range of mapping fields, including the geological map-

10.1016/j.ifacol.2021.10.123

ping of the seafloor with data acquired by bathymetric systems, morphological classification of regions via Benthic Terrain Modelling or even mapping of distinctive biological assemblages into biotopes. Benthic habitat maps are essential components of management plans designed to insure the sustainable use of the marine environment, and for the protection of fragile underwater ecology biomes. The ongoing developments of sonars and deep-sea imaging systems are progressively revealing the connections between benthic habitats and the seabed structure (Harris and Baker 2019).

2.2 Hydrography and underwater photogrammetry

By the means of metrology, hydrography and photogrammetry, are multidisciplinary branches of applied sciences which deal with the measurement and description of physical features remotely to analyse the shape, size, and position of targeted objects in a three-dimensional space. While hydrography mostly employs acoustic waves by measuring the travel distance of sent and received pings of eco-sounder (Lurton 2002), in photogrammetry light rays provide details on target structure, and given the appropriate equipment, may provide us with high-resolution, high quality images, which have additional information of colour and texture data not present in data delivered from sonar systems.

The basic concept of photogrammetry is to derive the shape, size and position of an area or object in space by remotely taken images of particular areas or objects from different angles. As a result, a three-dimensional reconstruction of the imaged object is possible using two-dimensional images. The derivation of the geometric quantities in space is subject to the central projective image and requires a reconstruction of the image ray bundles in three-dimensional space using the interior and exterior orientation of the camera. If these camera parameters are known or simultaneously calibrated, 3D object points can be (indirectly) determined from measured image points by spatial intersection, from which a 3D model of the captured object can then be constructed (Luhmann et al. 2019).

Underwater photogrammetry is more challenging due to the additional optical refracting interfaces, where the light rays travel through multiple medias, such as from waterproof camera housing (and the air inside), a glass lens, and seawater. The modelling of image rays through different media have been formulated in different environments, under the term of "bundle-invariant interfaces" (Luhmann et al. 2019). However, the water itself behaves as multi-media, variable in characteristics as a function of density, pressure, temperature and salinity, all of which can vary over short distances in the deep ocean. Therefore, an on-site camera calibration should be carried out immediately before, during or after image data acquisition. The transmission of sound and light differ in seawater. Acoustic wave travels well through water, and make remote sensing of objects possible. In contrast, light penetrates only relatively short distances through water. Depending on the water clarity, light can travel through the water column from centimetres to approximately a hundred meters. The attenuation of the light in the water is caused by absorption and scattering, which make the intensity of light decreases exponentially and gradually propagates through water with distance from the source (Open University Course Team 2001). That makes the acoustic wave the dominant tools in the deep-sea bathymetry compared to airborne photogrammetry and bathymetric LIDAR. However, in the clear water the result of close-range underwater photogrammetry shies by providing a sub centimetre high-resolution dataset to the end user, which is mentioned as micro-bathymetry in this study. The core of photogrammetry method employed for this study is based on Structure from Motion (SfM), which is a photogrammetric approach, which utilises the fully automatic extraction and matching of features resulting in fully automated orientation of images. In addition, most SfM programs allow for dense matching, meshing and orthophoto generation, which is a standard photogrammetric post-processing after bundle adjustment. SfM integrates a number of established methods, developed for non-targeted image data sets, to reconstruct a three-dimension structure or object in digital space from the motion of a camera (Kersten and Lindstaedt 2012; Luhmann et al. 2019).

2.3 OFOBS components and operation

Deep-tow observation platforms are ocean floor survey systems designed to operate in deep-sea environments, supplied with imaging systems and could be outfitted with sonars. These systems are submerged and towed behind a vessel at low speeds at the end of a cable measuring several thousand meters in length. The "Ocean Floor Observation System and Bathymetry" (OFOBS) is a deep-towed underwater imaging system (Fig. 1), property of Alfred Wegener Institute.

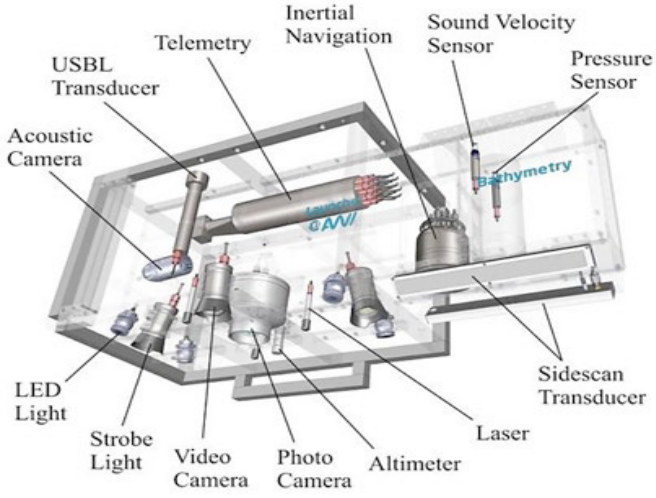

Figure 1. Schematic illustration of OFOBS instruments and components (Purser et al. 2018).

It is used for a variety of purposes, from bathyal organism observation to topographic/geological survey of hydrothermal activities within polar region. The main part is armed with two sets of camera systems. The high-resolution photo-camera is a Canon EOS 5D Mark III with a 24 mm fixed lens, which is mounted in a waterproof housing at the centre of vehicle. The second camera is a Sony FCB-H11 video camera for streaming and recording constantly during the whole dive via a RONIN HD-SDI system. The high-definition video camera is adjacent to the photo camera with a 5° tilt to the starboard side, in order to provide the best footage coverage together. Both of the cameras are mounted to a steel frame on the vehicle, accompanied

with two strobe lights, and three laser pointers at a distance of 50 cm from each other meant for dimension estimation of the seafloor structures and features. Moreover, four LED lights, supporting the lighting system and a USBL positioning system, enable to track the location of the OFOBS during deployments (Purser et al. 2018). Prior to PS101, the tow system was upgraded with a bathymetry extension, to expand the survey range of the vehicle in order to augment the seafloors pictorial data with sidelong swathes of habitat data provided by the side scan sonar (Boetius and Purser 2017). The main intention of deploying OFOBS to the height of several meters above the seafloor was to visually investigate the seafloor to determine the geological, sedimentological and biological community structures across the surveyed area. The benthic community structure on top of the Karasik Seamount was not well known prior to the PS101 expedition (Boetius and Purser 2017).

3. STUDY AREA AND HABITAT CHARACTERISTICS

The main expedition territory was in the region of 86°40'N and higher and 60° E. The Langseth Ridge seamounts included the large Karasik Seamount and the vicinal hydrothermal mount on the Gakkel Ridge rift valley (Fig. 2).

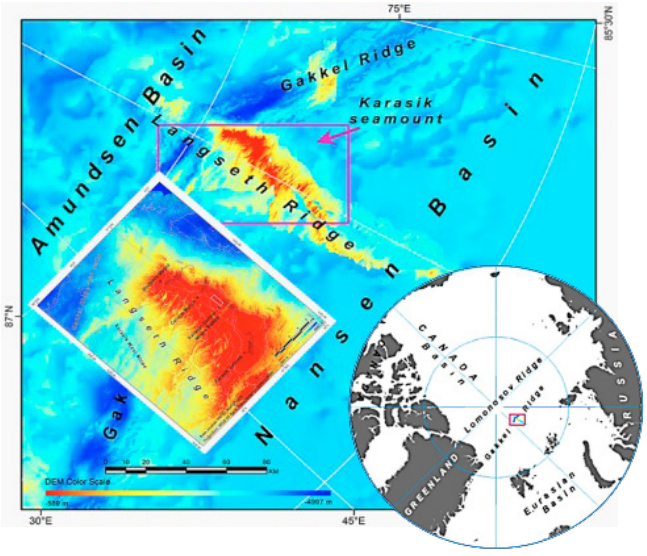

Figure 2. The map of the expedition area of PS101 and the study area (Shipborne multi-beam and IBCAO dataset)

The research area is located in the mid-Arctic Ocean, where the ocean is covered with year-round sea ice. During PS101 expedition, 15 OFOBS dives were successfully carried out. most of the dives were around the unofficially named Vent Mount of Gakkel Ridge Rift Valley and Karasik Seamount and toward the North Mount.

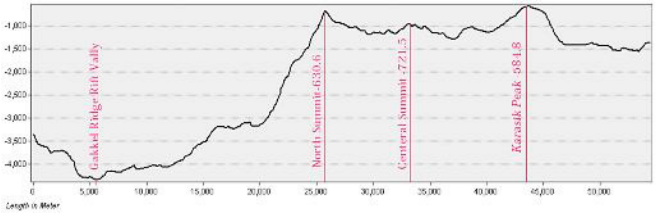

Figure 3. North-South profile of Karasik and vicinity peaks on Langseth Ridge.

The dataset used for this study is from the north part of the PS101/169-1 dive, which is located in the Central Mount along Langseth Ridge, north said of Karasik Seamount (Fig. 3). The OFOBS dive of Central Mount named as PS101/169-1 started on the Sep 30, 2016at 20:26 Coordinated Universal Time (UTC) and at the depth of -878 meter below mean sea level (86° 45.67' N ,061° 51.86' E). The total duration of the dive was 4 hours and 16 minutes and the length of the dive was 5,370 meter (Boetius and Purser 2017). The dataset used for this specific study was the last 500 meter of the dive, where the OFOBS towed from Karasik-central Mount Saddle toward the Central Mount summit.

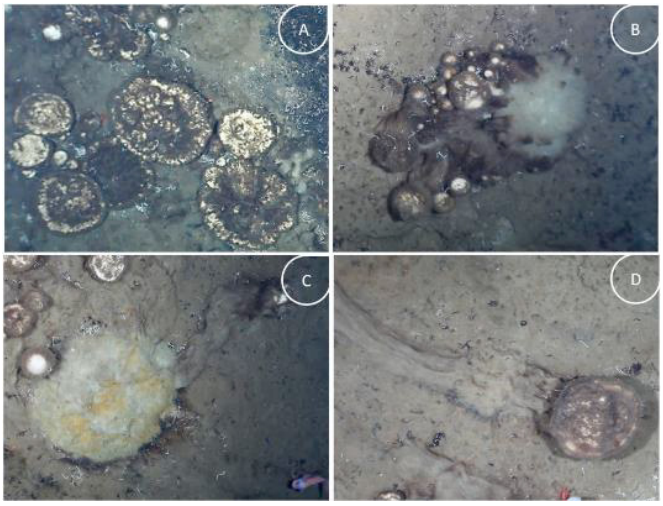

Figure 4. Diversity life stage of Geodia captured in OFOBS footage, (A) group of white-spotted sponges, (B) layer of bacteria mat and sponge spicules matte covered a group of sponges, (C) white-yellowish decaying giant sponge, (D) A Geodia spp. sponges and its track.

The OFOBS dives number PS101/089-01 revealed the typical habitat of the survey area of Karasik Seamount, which is the main dataset of this study (Fig. 4). The camera systems of OFOBS shows for the first time, a dense forest of sponges and sponge spines at the summit. There were several breaks in the sponge cover toward the northern section of the mount summit. The OFOBS footage are generally indicating a chaotic distribution of the sponges over the Langseth Ridge seamounts. In addition to that, there are white-spotted sponges in the scene, and white-yellowish microbial mats growing on decaying dead/dying sponges, spicules of sponges as well as sponge tracks on the seabed. In the surveyed area of the saddle and central mount, many other distinct fauna categories were also present in the cameras footage (Boetius and Purser 2017).

4. DATASET

The OFOBS datasets are categorized into three categories: sonar, imagery and navigation datasets. Some of the datasets have a dependency on the other instrument outputs. Specifically, the position strings of the OFOBS have several affiliations on other instruments such as shipborne GNSS and INS data which passed to the OFOBS IMU via a two way fibre optic communication cable. None of the sonar datasets of OFOBS has been employed for this study. However, the shipborne multi-beam bathymetry data is employed for mapping

purposes (Fig. 5). Both of the camera sets on board of the OFOBS were in operation simultaneously. The digital camera sensor provided a high-quality image of 22.3 megapixels (5760 × 3840 pixels) integrating important metadata from the positioning system, (time and position of image collection). The camera was automatically triggered with 20 seconds intervals, while manually shooting was possible by the operator. Simultaneously, the Sony video camera was streaming and recording in full HD resolution (1920 × 1080 pixels) with a rate of 25 fps during the whole dive. The idea of adding the video frames for 3D reconstructed model came up after the expedition was completed, to cover the seafloor gaps between the still images, with the SfM method in order to use the camera position for OFOBS navigation track correction. All unprocessed data is referred to here as "Raw data" including multi-sensor navigation data and imagery data sets. The first set of processes is meant to combine "Raw datasets" together, in order to enrich the position accuracy and the overall value of the geospatial and mapping material for the further process. The steps of the data preparation were developed during an earlier stage of the project for different OFOBS dive and are explained in detail (Dreutter 2017).

Figure 5. Data preparation for main process steps.

The distribution of the video frames and still images are neither equivalent in number or quality. In addition, the flight height of the OFOBS changed dramatically from 1 meter to larger than 5 meters, making the resolution of the relevant data more variable, which could be observed in the bathymetry data and the reconstructed 3D model. In addition, the still images area timestamped by the vessel GNSS timeserver in UTC via Posidonia USBL, and well fitted with the metadata file containing all available camera parameters. The data provided by both imagery systems are the main dataset for the reconstructed 3D model.

Enriched Raw Data: In order to fill the large gap between the high-resolution still images, the video frames are extracted in the rate of 1-4 fps (depending on the OFOBS FH and speed). The number of extracted frames could be increased or decreased to meet the minimum required overlap of 60%. In the next step, the timestamp of the still images and INS navigation/attitude data are synchronised and interpolated. At the end, the calculated values are assigned to the extracted video frames. By this process sequence, the raw video frames have been enriched by virtual interpolated metadata and then the enriched data sets are ready for the 3D reconstruction step. This part of preparation is adapted from a parallel study on OFOBS navigation correction, carried out in an earlier stage of the PS101 data processing stage (Dreutter 2017).

5. METHODOLOGY AND DATA PROCESSING

The methodology is designed to detect and extract the Geodia sponges and sponge spicules matte positions in the way that these could be measured and quantified across regions of seafloor, and could be applied for wet-biomass volume estimation thereafter. The process workflow is focused in 3D point cloud classification instead of direct object detection on raw images, since in most cases the Geodia sponges have very similar colour to seafloor beneath them, which is a big concern and challenge for the majority of feature detection algorithms. Fig. 6 gives an overview of the designed methodology. The sub-processes in the orange box are the main sponge detection part. The sections in the blue box illustrating the preparatory functions of the workflow where enriched data end up to a 3D model, which provide four different outputs. This include the camera positions, the dense point cloud, the mesh/DSM, and the orthophoto mosaic, which is the main dataset for sponge detection and wet-biomass estimation.

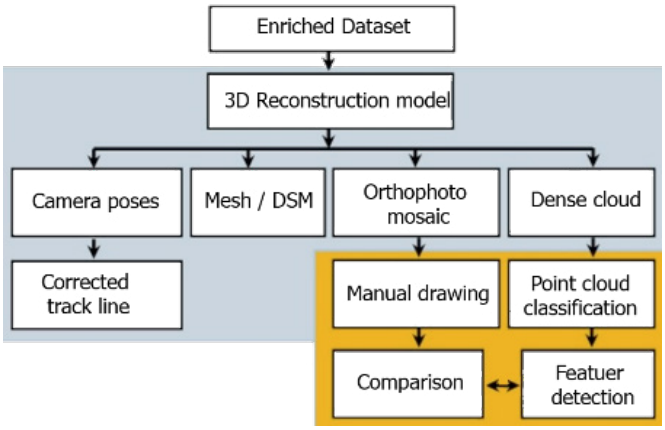

Figure 6. Overview of the data processing workflow

Each of these products employed to improve the imagery datasets, and used for the next step of classification.

5.1 3D model reconstruction

In the first processing step, SfM is employed to align the "enriched raw image data" including extracted video frames and still images, in order to reconstruct a continuous 3D model of OFOBS partial dive PS101/089-01. For this part of the process Agisoft PhotoScan software was used to align 1895 photos, where 5 % of them are high-resolution quality images and 95% are low quality interlaced video frames. Fig. 7 exemplary illustrates the coverage of the images.

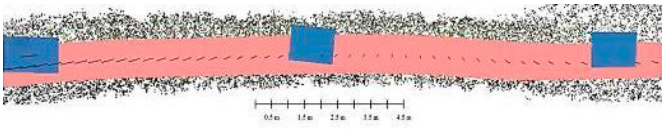

Figure 7. The coverage comparison of the still image (blue) and video frames (red).

Table 1. Basic information for the construction of a 3D model

Still images / video frames	95 / 1800
Aligned photos	1895
Tie points	756.365
Dense points cloud	103.256.691

The video frames were smudged by the movement and shaking of the OFOBS, which consequently affected the quality of the

point cloud as well. The Table 1 summarises the basic information for the construction of a 3D model.

5.2 Point cloud classification

The objective of point cloud classification is to use mathematical morphology to separate any points shaping biomaterial from the points shaping non-bio material, including sponges and sponge spicules accumulation. These two classes will be employed for sponge detection as well as biomass estimation.

Visual evidence from camera footage shows a complex environment, where it is hard to define specific boundaries between bio and non-bio materials. Within the sample area, the sponges have a very similar colour to the background seafloor as the seafloor in the sample area is covered with the sponge spicules mats. That's make it very difficult to detect and separate the sponges from the seabed background by using colour information. Therefore, an alternative separation factor should be defined to differentiate sponges from the seabed, though an uncertainty in identification should be expected. The data used for this part of the process is from the generated raw coloured dense cloud. Since the colour information is not involved in this process, henceforth it will be eliminated from the data. There are a few geospatial characteristics, which could be defined as the separation factor within the point cloud of the sample area, such as regional slope detected by angle or roughness. In order to define the change of angle in the near neighbourhood, as the first separation rules, a recently developed method was employed, namely the Cloth Simulation Filter (CSF) algorithm applied for DTM generation using point cloud classification. The algorithm is originally designed to extract ground points in LiDAR point clouds, but later developed and implemented for photogrammetry and remote sensing applications as well (Zhang et al. 2016). The CSF was applied as the first separation method, except for the ultra-noisy part of the sample area, where the result was not satisfactory and thus the backup method was applied. The roughness classification algorithm was also applied for the extracted unclassified point cloud section using the software CloudCompare (Girardeau-Montaut 2021). The aim of both point cloud classification methods is to separate non-ground points from ground points, which will be explained separately as follows.

Cloth Simulation Filter (CSF): This technique has two stages. The first step will divide the dense cloud into cells of a defined size where, within each cell, the lowest point is detected. Then the triangulation of these points provides the rough approximation of the terrain model. In the second stage, a new point is added to the ground class, which has to pass two conditions: firstly, it lies within a certain distance from the terrain model and secondly, the angle between the terrain model and the line to connect this new point with a point from a ground class is less than a defined angle. There is a loop repeating for the second step while there are still points to be checked. There are three parameters controlling the classification procedure: cell size, maximum angle and maximum distance. The cell size is determined by the size of the search window that the point cloud will be divided into as a preparatory step. The angle is one of the conditions to be checked while testing whether a point represents the seafloor. This parameter determines the assumption for the maximum slope of the surface within the scene. It sets a limitation for an angle between terrain model and the line that connects the point in question with a point from the ground class. The maximum distance parameter determines the assumption for the maximum variation of the ground elevation over a given time or distance. It is one of the conditions to be checked while testing a point as a ground point. It sets a limitation on the distance between the point in question and the terrain model.

Roughness Estimation: In the mid slope of the sample area, there is a 25-meter boundary, where the CSF algorithm result was not satisfactory, as a matter of the noise and therefore the low quality of the point cloud. Therefore, the alternative algorithm for classification applied, named as the Roughness estimation. This method was applied to the ultra-noisy area for DTM classification via CloudCompare tools. The surface roughness prediction model is based on a support vector machine and the logic of this method is to computes individual 'roughness' values per point with regard to its neighbour points. For each point, the 'roughness' value is equal to the distance between this point and the best fitting plane computed from its nearest neighbours. In cases where there are not sufficient numbers of neighbours to compute, (for example at the edges of the point cloud boundary,) the roughness cannot be found. In that situation a least-squares plane (LS plane) with invalid scalar values is used, where the adjacent neighbours are less than 3. The algorithm steps are described as follows: (1) the tool extracts neighbours around each point inside a sphere (kernel = sphere radius). (2) Then the tool fits a plane to the neighbours. At least three neighbours are needed but more points are recommended. (3) Finally, the tool computes the distance between the central point and the LS plane. The 'roughness' is then simply the deviation from the average local surface. To run the algorithm there is one variable which needs to be defined as "kernel size" which is the radius of a sphere centroid on each point. The right kernel value based only on the size of the features needs to be identified (Girardeau-Montaut 2021).

Visual detection: The georeferenced orthophotos are employed for the visual detection and manual drawing of the sponges in order to provide a reliable ground truth reference.

6. EXPERIMENT AND RESULT

Here we present the result of the experimented methods with the given parameter sets in the same order of the processing steps. First, the result and outputs of 3D reconstructed model and then the CSF point cloud segmentation over the flat and slop area are presented (Fig. 8), followed by the result of the Roughness Estimation for the ultra-noisy area over the slop.

6.1 Result of reconstructed 3D model

The 3D reconstructed model have several outputs for deferent used for deferent purpose The camera poses employed to improve the native navigation data for those disconnections between OFOBS and vessel positioning system, which caused multiple data loss for positioning and tracking. In addition, the camera positions considered as the flight height of the OFOBS in order to analysis the quality of uncleaned dense cloud. The DEM and orthophoto mosaic are employed for visual sponge

detection and manual drawing. The raw dense cloud is a multi-resolution point cloud which is not cleaned yet. The resolution and the density of the dense cloud is depended on the FH, and derivative of the Ground Sampling Distance (GSD). Within the sample area, the resolution of dense cloud varies from 3 mm to 9 mm. The other raster outputs, such as orthophoto mosaic and DEM inherit the property from the 3D model and are exported with the maximum possible accuracy of 3mm. The dense cloud is analysed and filtered for noise before the classification in order to detect sponges and wet-biomass, as two products of the point cloud, which is employed for further processing and geospatial data mining in another study (Mardani Nejad 2018).

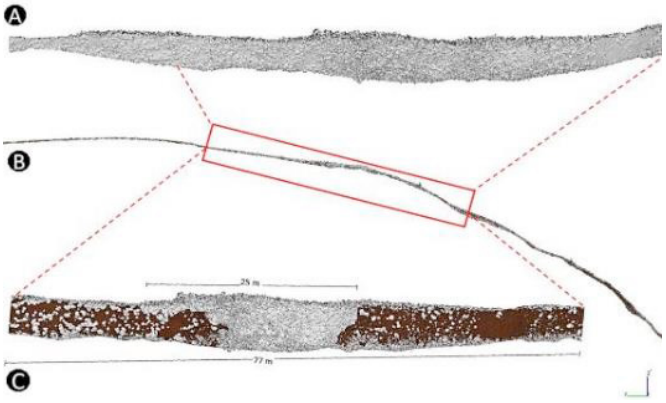

Figure 8. (A) Top view of the point cloud over the sloppy area (B) The side view of classified point cloud in the same area (C) The 25 m of the ultra-noisy area after classification. The grey areas are the unclassified points and the brown areas are the classified DTM points.

6.2 Result of Cloth Simulation Filter

For the CSF method, several different combination parameter sets applied, in order to classify the ground points (Table 2). The results of some of the given sets are illustrated in Fig. 9 for a small part of the sample area, which was mostly flat. The unclassified point in the datasets are considered as the sponges and sponge spicules matte.

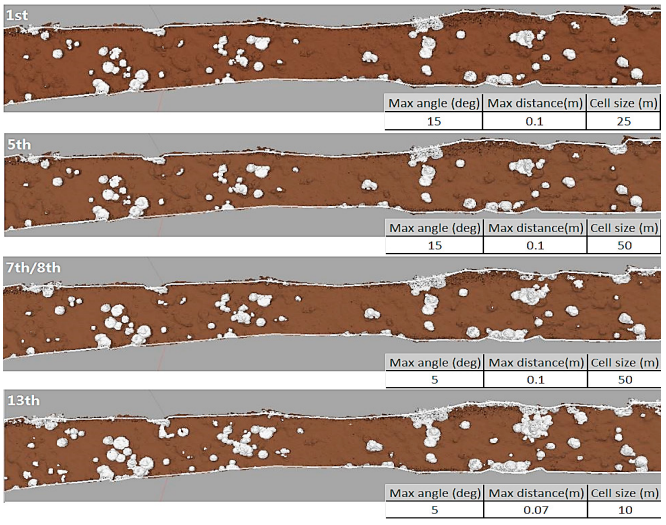

Figure 9. The result of CSF over the flat area for parameter sets 1st, 5th, 7th /8th and 13th.

Table 2. Parameter sets tested for dense cloud classification by CSF method. The highlighted rows are showing the convenient parameters for the flat (13th) and sloped (16th) area.

Parameter sets	Max angle	Max length	Cell size
1st	15°	0.1 m	25 m
2nd	15°	0.1 m	5 m
3rd	15°	0.2 m	5 m
4th	25°	0.1 m	5 m
5th	15°	0.1 m	50 m
6th	10°	0.1 m	50 m
7th	5°	0.1 m	50 m
8th	5°	0.1 m	25 m
9th	5°	0.1 m	10 m
10th	7°	0.1 m	10 m
11th	10°	0.07 m	10 m
12th	10°	0.07 m	25 m
13th	5°	0.07 m	10 m
14th	5°	0.06 m	5 m
15th	5°	0.05 m	10 m
16th	5°	0.05 m	5 m
17th	5°	0.05 m	2 m
18th	7°	0.05 m	2 m
19th	7°	0.05 m	1 m

The tested parameter set 13 shows acceptable output for the flat area. However, the CSF algorithm cannot deliver good results in the ultra-noisy area. On one hand, this is partly caused by the ground slope, and in the other hand it is partly the result of the OFOBS FH. Therefore, several parameter sets were applied specifically in this area, in order to get the best possible classification result. While different parameter sets improve classification result in the sloppy area, the classification result deteriorates in the flat area. As it is indicated in Fig. 10, the result of the CSF is not giving a similar output for the ultra-noisy area over the slope.

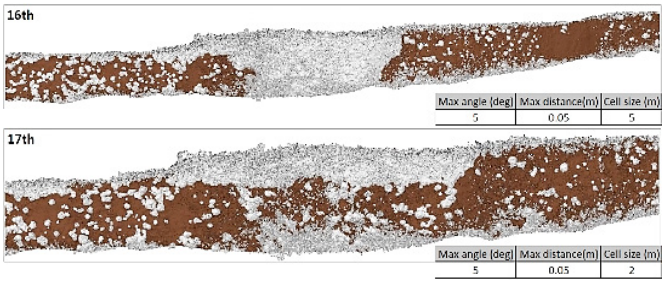

Figure10. The result of CSF over the slop for parameter sets 16th and 17th.

6.3 Result of Roughness Estimation

The remaining unclassified area has terrain slopes of about 35°, in addition to the cross-section slope of 25°. The OFOBS flight height during the survey jumped to 7.8 meter as a matter of crane height changes required by shipborne operations. All these factors caused low quality imagery with poor light condition on the seafloor and the production of an ultra-noisy

point cloud as well. The dense cloud of this area named as ultra-noisy area of the slope was classified with Roughness Estimation method. For the given point cloud, three different values are applied in order to get the best possible output by the experiment. As it is shown in Fig. 11, the kernel size of 3 cm, which is the default value of the exported dense cloud, does not provide a meaningful output. However, the two other tested values provide a better result. The kernel size of 100 cm, which is the approximate diameter of biggest sponges in the sample area, and the 35 cm, is the average diameter of most sponges in the sample area.

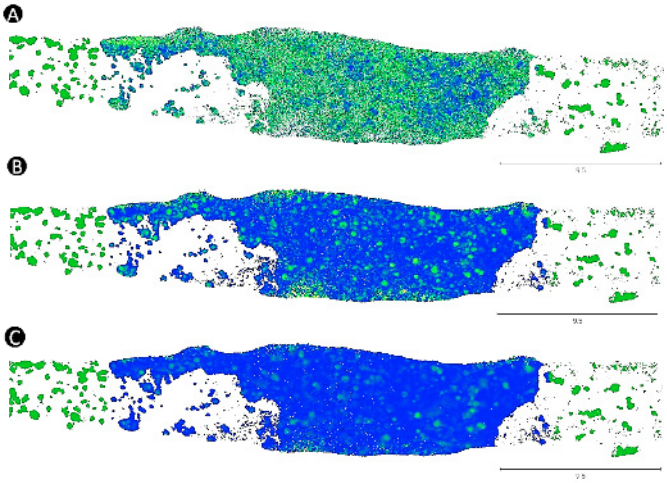

Figure 11. Outputs of Roughness estimation over ultra-noisy area. The kernel sizes are (A) 3 cm, (B) 35 cm and (C) 100 cm.

7. DISCUSSION

The images for the reconstructed 3D models are generated by two imagery systems. These distinct data sources are varying in properties and resolutions. They have a slightly different distance to the seafloor. Although it is almost impossible to implement the on-site camera calibration for such dynamic operation due to harsh environmental settings, therefore the triple downward-looking laser beam of OFOBS, employed as a pseudo ground control point in order to scale the final 3D model. Regarding the pixels number of each cameras image, the quality of the stills images are about 11 times richer than the extracted video frames (Fig. 12).

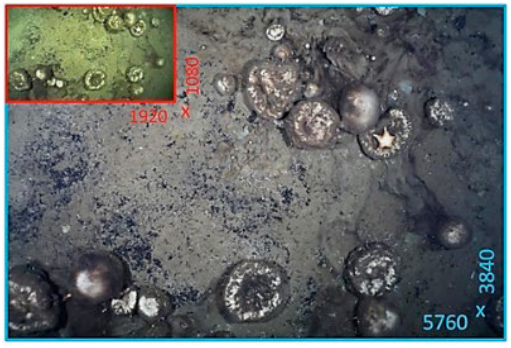

Figure 12. Compression of the full HD video frames (red) with 6K resolution still images (blue)

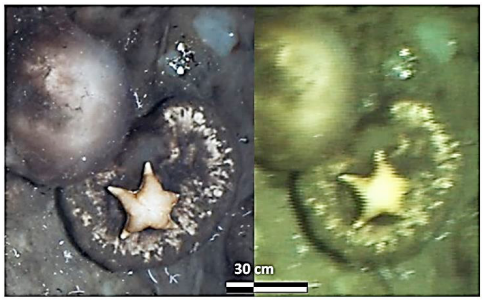

Figure 13. Compression of the quality of the still camera image (left) and interlaced video frames (right).

Regardless to dimension accuracy and location, the comparing of the two classification methods beside the visually detected sponges indicates the capacity of point cloud classification methods. The point cloud classification methods are superior to the manually detection in some area, due the colour similarity and low colour contrast of the sponges and the background seafloor (Fig. 14). This compression is valid mostly for those sponges, which are deteriorating. Meanwhile the visual detection is providing better results where there are several micro sponges are seating close to a giant sponge.

Figure 14. The example of the sponges, which are not easily detectable on visual detection due to low colour contrast.

The CSF is a time consuming process regarding the alignment and computation time in comparison to the Roughness Estimation method. Furthermore, the result of the CSF is not acceptable for slope areas. In addition, the FH of the OFOBS has direct impact on the coverage of camera footage linear and exponentially. On the contrary, FH has inverse impact on the imagery quality of the seabed and Ground Sampling Distance (GSD), as well as negative influence on the reconstructed 3D model. Thus, the point cloud classification accuracy and feature detection quality are indirectly depended on FH.

8. CONCLUSIONS

The nature of underwater photogrammetry and mapping projects require well-thought preparation such as camera setting and synchronization. For proper data acquisition, the manoeuvrability of the platforms in the hand of a skilled pilot plays a significant role in data quality and final results. The well-equipped ROV with stereo camera sets is a favourable example of an underwater photogrammetry survey, as it is demonstrated by Nornes et al. (2015). In the case of PS101 OFOBS dataset, the idea of 3D mapping and geospatial data mining developed after the data acquisition, which is not an usual approach for the mapping project. Therefore, a methodology is designed based on the existing dataset in order to map and de-

tect the Geodia sponges. The existing imagery dataset is enriched with video frames and native navigation data to enable data for mapping steps. The SfM is employed to produce micro-bathymetry data via reconstructing the 3D model of seabed. The DEM and orthophoto are used for visual detection while the dense cloud is employed for object detection. Both CSF and Roughness estimation are tested as point cloud classification methods over the micro-bathymetry data. The Roughness estimation method provides a better result over the sloppy area as well as the flat train. There are two major challenges in the dataset. First, the nature of the dataset, as mentioned before, a layer of spicules material covers the sponges and it is not possible to distinguish a boundary between them. Therefore, regardless to the material and consistency, all these variations considered as sponges, including yellowish bacteria accumulation or dead or dying sponges. This is one of the unsolved challenges for feature detection in point cloud as the designated method is dealing with non-coloured point cloud. The other challenge of the current dataset is low colour contrast of the sponges with the seabed background colour, since pattern recognition, algorithms benefit from high colour contrast within SfM and feature detection. In addition, there are two possibilities to improve the results. The major improvement is possible by providing more high-resolution still images. In addition, it is possible to boost the quality of the video frames by applying the de-interlacing process before 3D reconstruction step in order to reduce the noise caused by interlacing filter (Fig. 13).

REFERENCES

Boetius, A., and Purser, A. (2017). The Expedition PS101 of the Research Vessel POLARSTERN to the Arctic Ocean in 2016. Berichte zur Polar- und Meeresforschung = *Reports on polar and marine research*, Bremerhaven, Alfred Wegener Institute for Polar and Marine Research, 706, 230 p. https://doi.org/10.2312/BzPM_0706_2017.

Danovaro, R., Corinaldesi, C., Dell'Anno, A., and Rastelli, E. (2017). Potential impact of global climate change on benthic deep-sea microbes. *FEMS microbiology letters*, 364(23), fnx214. https://doi.org/10.1093/femsle/fnx214

Dreutter, S. (2017). Multisensor Microbathymetric Habitat Mapping with a Deep-Towed Ocean Floor Observation and Bathymetry System (OFOBS). Master Thesis, HafenCity University Hamburg, 2017.

Girardeau-Montaut, D. (2021). CloudCompare. http://www.cloudcompare.org/, last access 28 April 2021

Harris, P. T., and Baker, E. K. (2019). *Seafloor Geomorphology as Benthic Habitat: GeoHab Atlas of seafloor geomorphic features and benthic habitats*. Amsterdam: Elsevier, 936 p.

Keegan, B. F., Boaden, P. J. S., and Ceidigh, P. O. (1976). Biology of Benthic Organisms. *11th European Symposium on Marine Biology*, Galway, October, Pergamon Press, Oxford.

Kersten, T., and Lindstaedt, M. (2012). Automatic 3D Object Reconstruction from Multiple Images for Architectural, Cultural Heritage and Archaeological Applications Using Open-Source Software and Web Services. *PFG - Journal of Photogrammetry, Remote Sensing and Geoinformation Science*, 6, 727-740.

Luhmann, T., Boehm, J., Kyle, S., and Robson, S. (2019). *Close-Range Photogrammetry and 3D Imaging*. 3rd revised and expanded edition, Berlin, Boston: De Gruyter, 843 p.

Lurton, X. (2002). *An Introduction to Underwater Acoustics: Principles and Applications*. Springer Science & Business Media, 347 p.

Mardani Nejad, A. (2018). Benthic Habitat Analyses Using Micro-bathymetry Data and Subsea Photogrammetry. Master Thesis, HafenCity University Hamburg, 2018.

Nornes, S. M., Ludvigsen, M., Ødegard, Ø., SØrensen, A. J. (2015). Underwater Photogrammetric Mapping of an Intact Standing Steel Wreck with ROV. IFAC-PapersOnLine 48: 206–211.

Open University Course Team (2001). Chapter 5 - Light and sound in seawater. In: *Seawater. Its composition, properties and behaviour*, E. Brown (ed.), Oxford: Butterworth Heinemann in association with the Open University, 61-84.

Purser, A., Marcon, Y., Dreutter, S., Hoge, U., Sablotny, B., Hehemann, L., Lemburg, J., Dorschel, B., Biebow, H., and Boetius, A. (2018). Ocean Floor Observation and Bathymetry System (OFOBS): A new Towed Camera/Sonar System for Deep-Sea Habitat Surveys. *IEEE Journal of Oceanic Engineering*, 44(1), 87-99. https://doi.org/10.1109/JOE.2018.2794095

Zhang, W., Qi, J., Wan, P., Wang, H., Xie, D., Wang, X., and Yan, G. (2016). An Easy-to-Use Airborne LiDAR Data Filtering Method Based on Cloth Simulation. *Remote Sensing*, 8(6), 501. https://doi.org/10.3390/rs8060501

The data used in this paper is available at the PANGAEA archive of the Alfred-Wegener-Institute, Helmholtz Centre for Polar and Marine Research (AWI). In order to access the data, please contact the following e-mail address: info-bathy@awi.de.